Simple Shear Deformation of Polypropylene via the Equal Channel Angular Extrusion Process

Andrew Phillips,* Peng-wei Zhu, and Graham Edward

Department of Materials Engineering, CRC for Polymers, Monash University, Vic 3800, Australia

Received April 4, 2006; Revised Manuscript Received June 18, 2006

ABSTRACT: The morphological changes of isotactic polypropylene (iPP) subjected to varying shear strains have been investigated by the equal channel angular extrusion (ECAE) process. Morphological measurements were made by wide- and small-angle X-ray scattering (WAXS and SAXS) using synchrotron radiation, differential scanning calorimetry (DSC), and reflected optical microscopy (ROM) of permanganic etched specimens. ROM results reveal the initially equiaxed spherulites are elongated with increasing shear. The deformation of the spherulite was found to always lag behind the overall macro deformation. This was attributed to the interlocking nature of the α spherulites. WAXS and SAXS results revealed two preferred crystallite and crystalline *c*-axis orientations at all shear strains investigated. In both orientations the crystalline *c*-axis was found to be incorporated along the length of the crystallite. It is proposed that the observed scattering was due to the formation of two microfibrillar domains.

Introduction

Over the years a significant amount of work has been devoted to understanding the solid-state deformation of semicrystalline polymers above the glass transition temperature. The vast majority of the work has focused on the tensile mode. More recently, authors have investigated the shear[1−5] and compression[6−9] modes. The study of shear deformation is of particular interest as not only is it a basic mode of deformation at the microscopic level, but it also could be used to create high orientation throughout a large cross section of polymer material. Highly oriented polymers are well-known to exhibit enhanced mechanical properties.

The equal channel angular extrusion (ECAE) process has been identified as an advantageous method of inducing bulk simple shear into materials. The process consists of two rectangular channels of equal dimension meeting at a sharp bend of angle Φ (Figure 1). A billet is placed into the top chamber and pushed by the action of a plunger through the channel, around the bend and into the second channel. Examination of the deformation process under zero-friction conditions shows that simple shear occurs over a narrow zone and is uniform throughout the billet.[10−12] It has been used to attain controlled large-scale plastic deformations in many polymer systems such as LDPE, HDPE, iPP, PC, and PET.[13−20] More recently, ECAE has been applied to glass fiber/polyacetal composites[21] and clay/nylon-6 nanocomposites.[22,23] In all these polymer systems and polymer composites it was considered that significant molecular and second-phase fiber orientation was induced into the billets after processing. The advantages of ECAE for studying shear deformation are (a) it promotes uniform structure and property development throughout the extruded billet and (b) large deformations are possible without a decrease in work-piece cross-sectional area.

Various authors have studied the evolution of morphology of polymers subjected to shear deformations. However, as yet no one study has been done to elicit the morphology evolution in one polymer system, at the spherulite through to the molecular scale, from small to large shear strains. At low shear strains

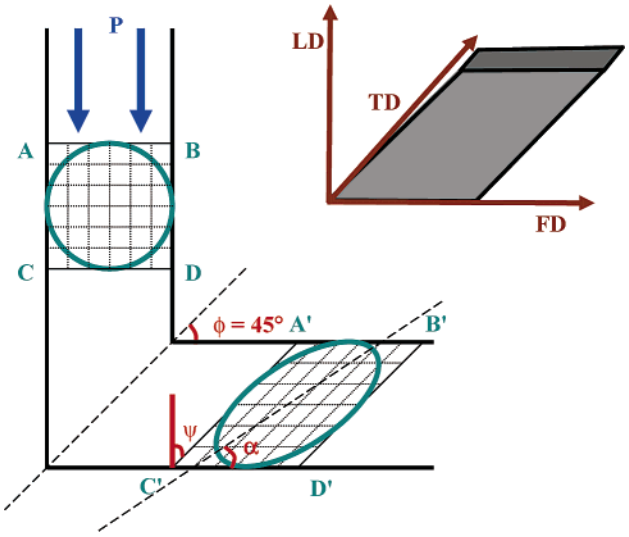

Figure 1. Schematic of the experimental setup of the ECAE die showing the ideal deformation of a billet.

$\gamma = 0-1.2$ the initially equiaxed spherulites in iPP form ellipsoids.[3] At higher shear strains γ approaching 2.0 in LLDPE[13] and PET[18] the spherulite morphology is destroyed, replaced by macrofibrils aligned along the principal tensile axis. X-ray diffraction studies of PET,[18,20] HDPE,[2,4] and iPP[14] revealed a bimodal distribution of molecular *c*-axis and crystallite normal orientation. Argon et al.[2] proposed that the formation of this bimodal orientation was due to the simultaneous action of the chain slip and interlamellar shear mechanisms, each leading to the occurrence of a preferred lamellar orientation. Xia et al.[18] explained the origin of this preferred orientation by the selective deformation of crystalline areas within a spherulite.

In this research, billets of iPP were subjected to simple shear at room temperature via the ECAE processes. The purpose of this work is to investigate the morphology evolution, from the spherulite through to the molecular scale and from small to large shear strains. The likely mechanisms of deformation as well as the origin of the preferred crystalline orientation will be discussed.

* Corresponding author: e-mail andyphil@alphalink.com.au.

10.1021/ma0607618 CCC: $33.50
Published on Web 07/21/2006

Experimental Section

Square sheets (150 mm × 150 mm × 10 mm) of the iPP homopolymer HP400N were compression-molded from pellets at 210 °C for 15 min and furnace-cooled to room temperature. The ECAE die used in this investigation had a channel cross section of 10 mm × 20 mm, where the corners are on the narrower 10 mm edges. Billets with dimensions 50 mm × 20 mm × 10 mm were machined from the square sheet. It has been found in the past that scoring lines on the outside of ECAE billets to quantify the shear strain caused shear to become localized along the score lines.[14] This undesirable effect was overcome by drawing a square grid (5 × 5 mm) on the inner surface of a representative billet which had been cut in half and then put back together before extrusion.

Billets were extruded through the 90° equal channel die at room temperature, with no lubricant, at a constant velocity of 2 mm/min in a screw-driven Inston 5500R. Three directions that describe the geometry of the billet after processing are flow direction (FD), load direction (LD), and transverse direction (TD) (Figure 1). To increase the level of shear strain, previously extruded billets were reinserted into the die for a second pass in the same orientation as the previous pass. Tensile specimens were machined from the compression-molded sheet and uniaxially drawn at 2 mm/min to a strain of 15% and then at 10 mm/min to failure. A tensile yield stress of 27.8 MPa, a modulus of 1.2 GPa, and an elongation at break of $\epsilon = 6.9$ were recorded. This provided an example of a highly oriented morphology.

It has been shown by Aboulfaraj et al.[24] that the crystallization kinetics vary across the thickness of compression-molded sheets due to the temperature gradient between the two external surfaces. This results in the spherulitic structure being thickness dependent. Therefore, all specimen analysis was performed on material taken from the geometric center of the original compression-molded sheets.

The simultaneous wide- and small-angle X-ray scattering experiments (WAXS and SAXS) were performed at room temperature at the Australian National Beamline Facility (ANBF), a synchrotron beamline at the Photon Factory in Tsukuba, Japan. A multiconfigurational vacuum diffractometer was used for X-ray experiments. Details of the experimental setup of the diffractometer have been reported in previous papers.[25,26] Beam dimensions were 200 μm × 200 μm, the exposure time was 600 s, and the wavelength was 2 Å. The camera lengths for SAXS and WAXS were 570 and 110 mm, respectively. Scattering without the specimen was also recorded to enable background correction of the WAXS and SAXS patterns.

Differential scanning calorimetry (DSC) experiments were performed on a Perkin-Elmer DSC-7 at heating rates of 10 °C/s and under a nitrogen atmosphere. Sample size was ~10 mg. Pure indium and zinc references were used for calibration. Enthalpy of fusion, ΔH, was determined by integrating the area under the baseline corrected thermogram between 130 and 175 °C. Percentage crystallinity was calculated from the ratio of $\Delta H/\Delta H_0^{iPP}$, where ΔH_0^{iPP} for 100% iPP was taken as 148 J/g.[27,28]

To observe changes in the spherulitic microstructure, the permanganic etching technique first proposed by Olley[29,30] and later refined by Park[31] was used. Smooth surfaces of the material to be examined were prepared by microtoming at room temperature with a glass knife. These were immersed in a vigorously stirred solution of 3 wt % $KMnO_4$, 64.7 wt % concentrated H_2SO_4, and 32.9 wt % H_3PO_4 for 7 h. After etching, specimens were quenched into cold hydrogen peroxide and washed in an ultrasound bath to remove any artifacts caused by the etching procedure. Reflected optical micrographs (ROM) of etched surfaces were taken in an Olympus PMG3 microscope with a differential interference optic attachment.

Results

Observations on the Macroscopic Scale. Figure 2 shows the deformation induced into the billets after one and two passes. After one pass a large area of reasonably constant shear strain was observed in the middle of the billet. Near to both free surfaces the shear strain dropped off considerably and remained reasonably constant until the edge is reached. A closer examination of shear strain vs distance across a typical billet after one pass was performed with the aid of the tracing program DATATHIEF (Figure 2c). This showed the length of the low-shear region was larger at the bottom ("outside" at the corner) of the billet than at the top ("inside"), being 2.0 mm as compared to 0.5 mm.

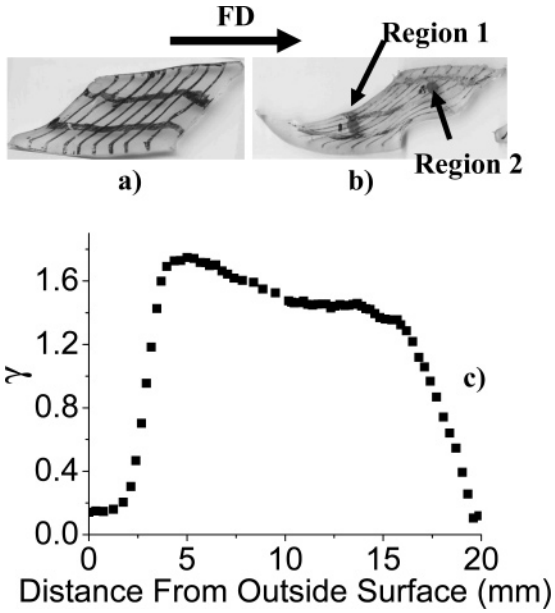

Figure 2. ECAE billet after (a) 1 pass and (b) 2 passes and (c) distribution of shear strain across billet after 1 pass.

The shear strain induced into the billet after two passes was not as uniform as after one pass; however, at small scales the shear strain was relatively uniform. Reextruding the billet allowed a maximum shear strain of 3.1 to be obtained near the outside of the specimen, region 1, and a smaller shear strain of 2.4 near the inside of the specimen, region 2.

The variation in shear strain found in both 1 and 2 pass samples provided a unique opportunity to examine material processed in the same way but exposed to varying degrees of shear. Using appropriately calibrated samples, representative material was extracted from ECAE processed billets for morphological examination. At the small scales examined the variation in shear strain across an individual measurement area due to the shear gradients is small, and the material can be considered homogeneous.

Observations on the Spherulite Scale. The series of micrographs in Figure 3 shows the evolution on the micrometer scale of iPP subjected to increasing shear strain. Initially, the microstructure consists of uniform equiaxed spherulites which are composed of long fibrous ribbons radiating out from a central point. As these spherulites formed in the absence of concurrent deformation, it is expected that they will be the monoclinic α modification.[32] X-ray and DSC measurements taken on the undeformed sample confirmed this. As the shear strain is increased, the spherulites began to transform into ellipsoids with their major axis being inclined to FD. This angle tended to rotate further toward FD with increasing shear strain. Interestingly, the angle of inclination of the major axis of the elliptical spherulites was found to always lag ~20° behind the direction of maximum principal strain.

At intermediate shear strains ($\gamma = 1.3-1.5$) the spherulite morphology appeared to be totally destroyed looking down TD. What was left is a fibrous texture which is roughly aligned along

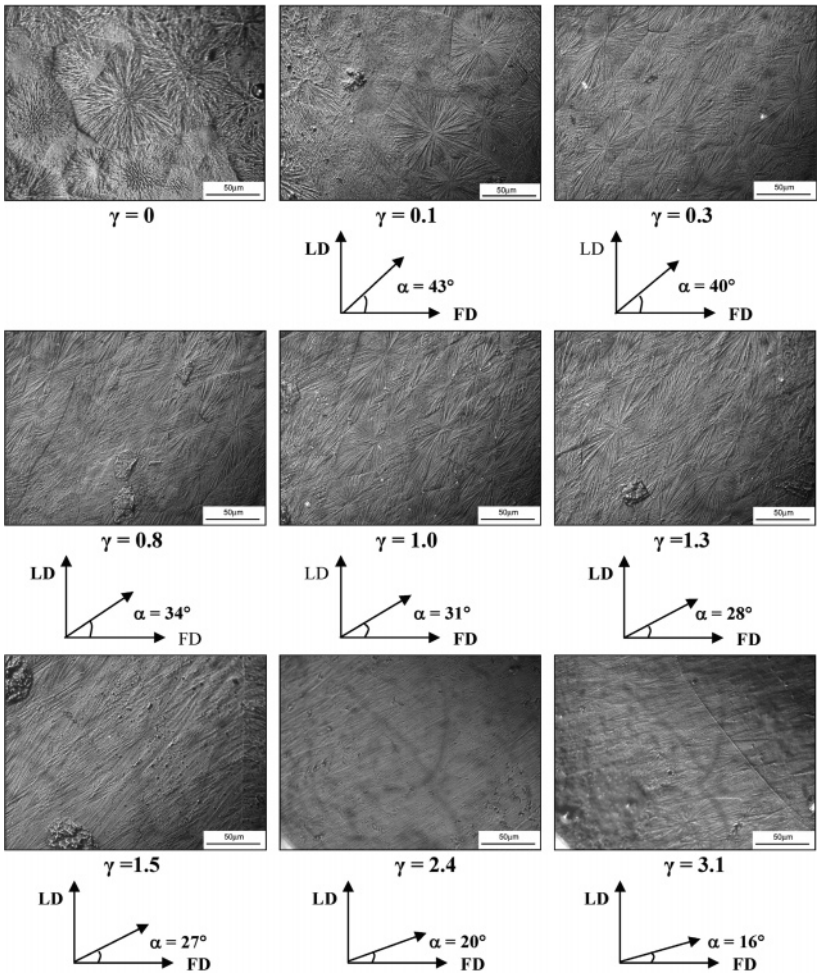

Figure 3. ROM of permanganate etched specimens subjected to varying degrees of shear strain.

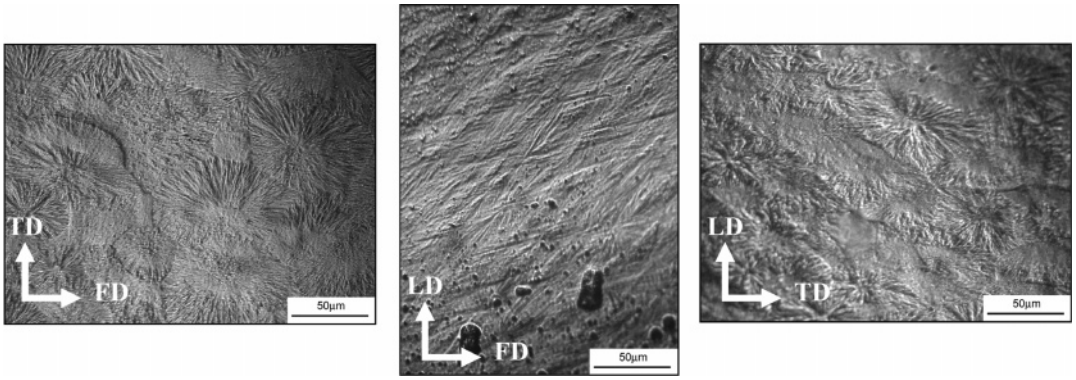

Figure 4. ROM of permanganate etched specimens sectioned normal to the three axes LD, TD, and FD at $\gamma = 1.5$.

the direction of maximum tensile strain. However, when looking down either FD or LD, some spherulites still appear to remain intact (Figure 4). When viewed along LD the remaining spherulites were found to be elongated along FD. Equiaxed spherulites where found when viewing along FD. In both FD and LD directions the remaining spherulites appeared to be more fragmented compared to the undeformed spherulites, and some regions were totally devoid of spherulitic structure. Apparently, the elliptical spherulites become so thin that they do not discernibly retain their spherulitic structure when looking down TD. However, they do retain their spherulitic structure looking down LD and FD, and so they may be pictured as elliptical lamina shapes, with their plane and long axis aligned with the direction of maximum tensile strain.

At the highest shear strains investigated ($\gamma = 2.4-3.1$) the angle of the fibrous texture was still aligned along the direction of maximum tensile strain. At a shear strain of 3.1 the fibers are inclined at about 16° to FD. At these higher shear strains the contrast revealed by the permanganate etchant was significantly lower than that found for the lower shear strains. The most likely cause of this low contrast is the refinement of microstructure produced as a result of the deformation.

Observations on the Molecular Scale. Figure 5 shows 2D X-ray diffractograms of an undeformed (isotropic) and a highly oriented cold drawn sample for comparison. For clarity, the SAXS region was enlarged relative to the WAXS region. In the case of the cold drawn sample the drawing direction was to the right. Before deformation the lamellae and molecular *c*-axis

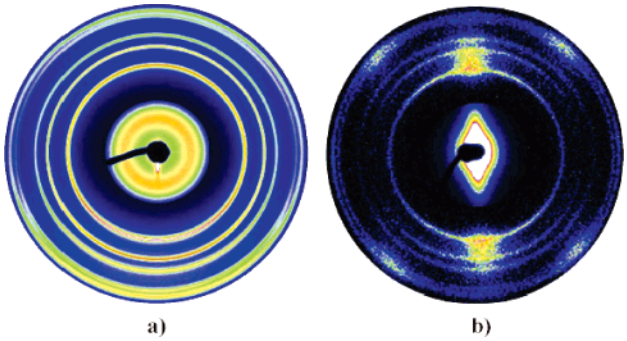

Figure 5. 2D X-ray diffractograms of (a) undeformed and (b) highly oriented cold drawn iPP. Drawing direction is to the right. Note for clarity the small-angle region has been enlarged relative to the wide-angle region.

distributions were found to be isotropic. The X-ray diffractogram of the cold drawn sample shows the well-known fiber pattern.[33−35] Concentric circles found in the wide-angle region of the undeformed material have contracted to small spots occupying a small azimuthal angle. This is characteristic of the crystalline portions of the semicrystalline sample having their *c*-axis (molecular chain helix axis) oriented along the drawing direction. The broad concentric ring found in the small-angle region of the undeformed sample has transformed into sharp lines in the meridional position. This can be explained by the formation of a microfibrillar structure aligned along the drawing direction.

X-ray diffraction experiments were performed on material taken from the center of a billet after one pass, corresponding to a shear strain of 1.5 and where the X-ray beam was parallel to each of the three defined axes TD, FD, and LD (Figure 6). The most interesting view is when the X-ray beam was parallel to TD and FD was to the right. In the small-angle region two distinct sets of lobes were found: one in the meridional position and one inclined ∼27° to the meridional line. In the wide-angle region the sharper concentric rings had become more intense in two azimuthal directions. This bimodal *c*-axis orientation of the crystallites and the crystallite normals has been observed before in other semicrystalline polymers subjected to simple shear.[2,14,18]

The LD view revealed there was a general increase in crystalline *c*-axis orientation along FD as a result of the simple shear deformation. A general increase in the orientation of the crystallite normal along FD was also observed, as shown by an increase in relative scattering intensity in the equatorial region. Interestingly, it appears that this increase in scattering intensity is due to the formation of a lobe of minimum scattering intensity in the meridional position rather than a lobe in the equatorial position.

Viewing along FD the scattering intensity was significantly less than the other two directions, and no discernible crystalline *c*-axis orientation could be observed. This suggests significant *c*-axis orientation along FD. A sharp increase in the scattering intensity in a narrow band in the meridional position of the small-angle region signifies the presence of microfibrils.

To probe the evolution of crystalline morphology with increasing shear strain, 2D X-ray diffractograms were taken at

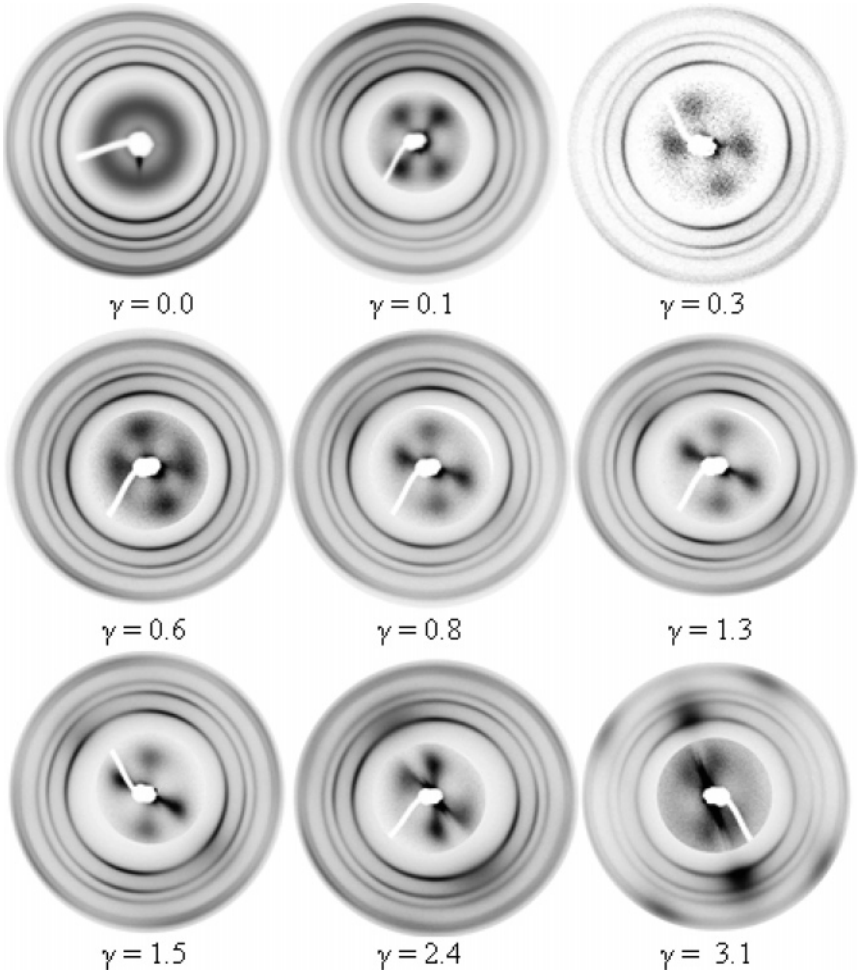

Figure 6. 2D X-ray diffractograms of material subjected to varying degrees of shear strains looking down TD and where FD is to the right. Note for clarity the small-angle region has been enlarged relative to the wide-angle region.

various locations with different shear strains, in all cases looking down TD and where FD was to the right. The results are shown in Figure 6. Again for clarity the SAXS region is enlarged relative to the WAXS region. Even after a small amount of shear strain has been induced into the material the distinct bimodal orientation is observed. In the small-angle region two lobes were formed about 40° either side of the meridional line. In the wide-angle region the scattering intensity increases in two azimuthal directions. Furthermore, the direction of the low order reflections appears to be closely aligned with the directions of the lobes.

It is clear looking at the data for higher shear strains that this trend continues and that the scatterings of the small- and wide-angle regions are intimately linked. To assist in the discussion, two orientation domains can be defined, C_1 and C_2, where C_1 is aligned 40° clockwise and C_2 is 40° anticlockwise from the meridional line at $\gamma = 0.1$. With increasing shear strain it can be seen that the angles of inclination of C_1 and C_2 rotate clockwise. Both domains initially rotate quickly but then slow down when they approach the meridional line. As the strain increases, the degree of orientation of both domains is also seen to increase. Additionally, the intensity of the C_1 domain increases relative to C_2 as the shear strain is increased.

At the highest shear strains investigated the two lobes in the small-angle region begin to fade. They are replaced with a single sharp line of scattering between them at an angle of ~15° to the meridional line. In the wide-angle region the two peaks in azimuthal intensity also begin to disappear and are replaced with a single peak aligned in the direction of the new peak in the small-angle region. This new scattering is characteristic of microfibrillar formation.

To further probe the crystalline evolution of polypropylene with increasing degrees of shear deformation, the volume crystallinity as well as the crystallinity aligned along each preferred orientation was estimated. A volume crystallinity index, χ_v, for each specimen was calculated by separating the amorphous and crystalline contributions to scattering between $1 \le r(2\theta) \le 12$ and $0 \le \phi \le 360°$ (i.e., around the ring from 5 to 18 2θ). The amorphous contribution, A_A, was determined by fitting a Gaussian-shaped curve to 30 points selected to define the shape; the crystalline contribution, A_c, was determined by integrating the scattering above this amorphous halo. To allow integration around the scattered rings, the Cartesian $x-y$ coordinate 2D WAXS and SAXS patterns were transformed into polar $r-\phi$ coordinates. This method ignores contributions from the degree of crystal perfection as proposed by Ruland;[36] however, this was not considered important for comparisons within one grade of material. The volume crystallinity index was then estimated by

$$\chi_v = A_c/(A_c + A_A) \quad (1)$$

In a similar way crystallinity measurements were also performed along each preferred orientation domain C_1 and C_2 over an arc of width $\phi = 5°$. The crystallinity of each domain were denoted χ_{c1} and χ_{c2}, respectively.

Figure 8 shows that the volume crystallinity index of the samples decreases roughly in proportion to the amount of shear strain. Initially, the material had a volume crystallinity index of 54%. After ECAE processing to the maximum shear strain of 3.1, the crystallinity had dropped by almost half to 28%. This shows that crystalline order is being destroyed continually throughout the deformation process. The volume crystallinity was measured for the cold drawn specimen to act as a comparison for a different mode of deformation (tensile). The crystallinity of the cold drawn specimen, which had been subjected to $\epsilon = 6.9$, was determined to be 39%. This shows that shear deformation is perhaps more effective at destroying crystalline structure than tensile deformation, although the contribution of strain-induced crystallization would also need to be considered. Further analysis was performed on the crystallinity of each preferred orientation. The C_1 crystallinity was found to be lower than the C_2 crystallinity, suggesting that C_1 crystallites are destroyed more easily by the deformation than C_2 crystallites.

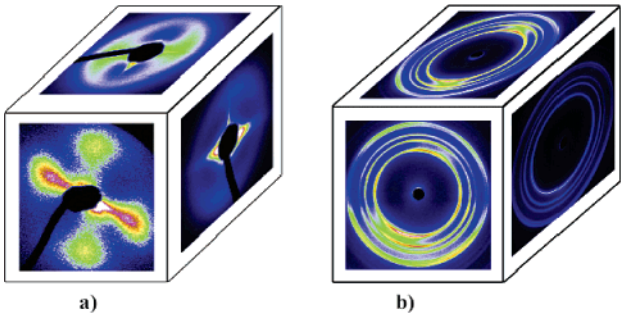

Figure 7. 2D X-ray diffractograms viewing along the three principal axes LD (vertical), TD (in/out of page), and FD (horizontal). (a) SAXS; (b) WAXS.

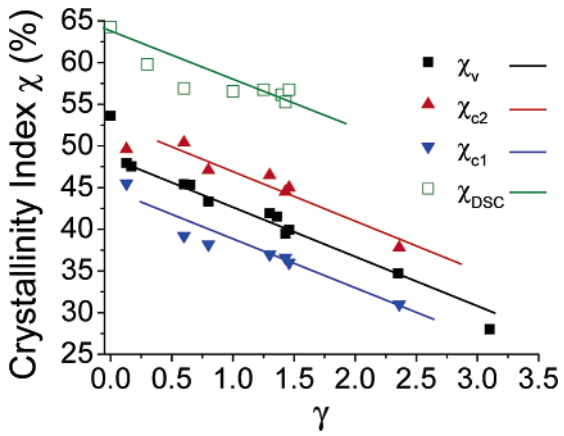

Figure 8. Plots of volume crystallinity index and crystallinity index for each preferred orientation as a function of shear strain.

To confirm the X-ray crystallinity findings DSC experiments were performed, and the results are shown in Figure 8. Within experimental uncertainty the crystallinity as measured by DSC (χ_{DSC}) decreased in roughly the same manner to the crystallinity as measured by X-ray. In these DSC experiments uncertainty arises, especially at lower shear strains, due to the difficulties in obtaining representative material in the shear gradient region. The difference in the absolute value of crystallinity between X-ray and DSC can be explained on the basis of the ΔH_0^{iPP} value used to calculate crystallinity from the DSC endotherm. A quick search of the available literature reveals ΔH_0^{iPP} values ranging from the value used in this experiment 148 J/g to 138 J/g[37] to 168 J/g.[38,39]

Discussion

Structural Background. Natta[40] showed that the usual monoclinic α crystal form of iPP has each polymer molecule arranged as a 3_1 helix. In the crystals, bonding along the chains is covalent while bonding between chains is van der Waals bonding. This causes the tensile modulus perpendicular and transverse to the chain to differ by some 2 orders of magnitude. The polymer chains fold back and forth on themselves to form crystalline lamellae.[41] These lamellae form long ribbons which

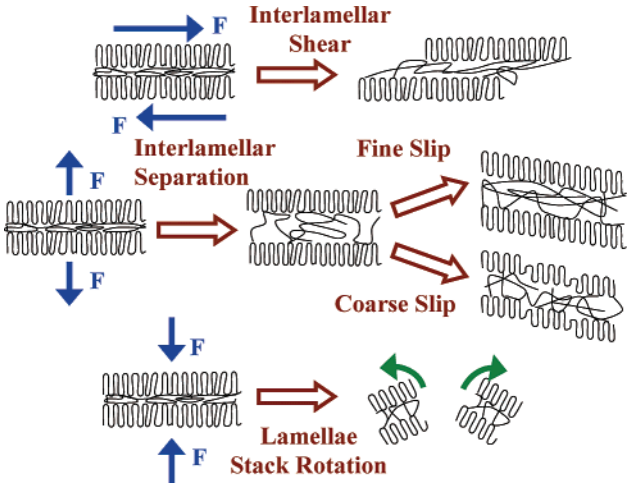

Figure 9. Plastic deformation mechanisms in semicrystalline polymers $T_g < T_m$.

are twisted about their molecular axis.[42] The lamellae and ribbons are connected by tie chains which are incorporated into adjacent lamellae and ribbons. The interlamellar and interribbon region is amorphous and consists of tie chains, chain ends, loose loops, and unincorporated ends. The long ribbons radiate out from a central point and form a spherulitic structure.

In iPP formed without concurrent deformation the major crystalline phase is the monoclinic α modification. α spherulites contain two families of lamellae: radial or parent and tangential or daughter lamellae.[43] In the case of parent lamellae, crystallites grow along the radius of the spherulite, and their growing direction coincides with their *a** direction. Daughter lamellae, on the other hand, grow epitaxially on the parent lamellae. The *a** direction of the parent lamellae matches the *c*-axis direction of the daughter lamellae. Compared with parent lamellae, the daughter lamellae are small and imperfect, and the size of the daughter lamellae is nonuniform. Parent and daughter lamellae are linked together by tie molecules, and a certain portion of the tie molecules remain entrapped between the two lamellae in the amorphous region.

Prior to yielding, deformation of semicrystalline polymers is accomplished primarily by the deformation of the amorphous phase, which is rubberlike. Bartczak et al.[8] suggested that the most important deformation mechanism in the amorphous region of semicrystalline HDPE is the glide of chain segments along their axes analogous to the chain slip observed in the crystalline part of the polymer. Depending on the location of individual lamellae within the original spherulite and the lamellae's orientation relative to the applied stress, three deformation modes have been postulated:[44] shear of the amorphous phase (interlamellar shear), stretching or compression of tie molecules (interlamellar separation and compression), and rotation of lamella within their soft amorphous matrix (lamella-stack rotation).

At the yield point, the polymer chains in the amorphous region find it increasingly difficult to slide past each other, and continued deformation of the polymer results mainly from the crystalline phase. Polymer crystals can deform by slip, twinning, or strain-induced martensitic phase transformations.[44] Twinning and strain-induced martensitic phase transformations have been observed in other semicrystalline polymers such as PE. The mechanism is considered to contribute little to the overall plastic strain[45] but may intervene to bring crystals into a more favorable orientation for slip.[3] Figure 9 summarizes the key deformation mechanisms in semicrystalline polymers.

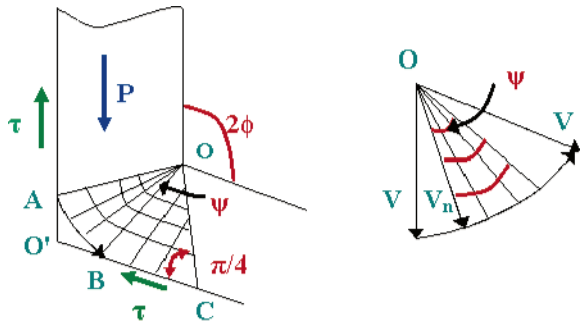

Figure 10. (a) Slip line field and (b) corresponding velocity hodograph with equal friction in both channels (ref 11).

Because of the high strength of the covalent bonds along the chain axis compared to the relatively weak van der Waals bonds between adjacent chains, it is energetically unfavorable that the slip plane will cross the chain direction. This leads to the slip guide plane being of the {*hk*0} type; i.e., slip occurs either parallel or perpendicular to the chain axis. Like most ductile crystalline materials plastic flow in semicrystalline polymers is governed by the nucleation and motion of dislocations on slip planes. It is widely accepted that pure screw dislocations are generated from the edges of crystalline lamellae.[46,47] Furthermore, chain slip in the same kind of plane can occur in two different ways to accommodate the same overall macroscopic deformation: fine and coarse slip. Fine slip usually occurs at small strains equally on a large number of parallel planes, resulting in a change in the angle between the chain axis and the normal to the lamellae surface. Coarse slip occurs at larger deformations on a few parallel planes, resulting in the fragmentation of lamellae into blocks which thus slide past each other. The angle between the chain axis and the normal to the lamellae surface does not change significantly.[3]

Shear Deformation on the Macro Scale. It can clearly be observed that the ECAE process is very effective at inducing large degrees of shear deformation into bulk specimens. After one pass the maximum shear strain recorded was $\gamma = 1.5$. After two passes the shear strain was increased to a maximum of $\gamma = 3.1$. The experimentally obtained shear strains were reasonably close to the theoretically obtainable shear strains of $\gamma = 2$ and $\gamma = 4$ after one and two passes. That the observed shear strains are lower than ideal is caused by a combination of nonzero friction at the polymer die interface and elastic bending around the 90° corner. Elastic bending can be reduced by applying more backpressure, and the overall process can be influenced by changing the temperature of deformation. It is likely that the orientation could be improved by increasing the temperature of processing, but that aspect of the process was not considered here.

Friction at the die/polymer interface creates a center fan field originating at the inside corner (OAB), as described by Segal[11] (Figure 10). A center fan field leads to the formation of a dead metal zone O′AB, which then leads to the nonuniform strain pattern observed across the billet. This less than ideal situation gave an unexpected benefit for this work in the form of a shear strain transition region near the surface of billet which could be utilized to study the evolution of microstructure under simple shear.

Shear Deformation on the Spherulite Scale. While the spherulite boundaries remained intact, it was observed that the spherulite deformed less than the overall macroscopic deformation. The angle of the major axis of the now elliptical spherulite lagged ~20° behind the principal strain axis. Aboulfaraj et al.[5] observed the same phenomenon in an ~50% mixed α and β

modification material subjected to simple shear. They found that the α spherulites deformed 25% less and the β spherulites deformed 25% more than the macro deformation. They explained this in terms of the interlocking nature of the tangential lamellae found in the α spherulites providing structural resistance to the deformation. The β spherulites then made up for the more rigid α spherulites by deforming more, thus accommodating the overall deformation.

In this work the crystalline part of the material is composed virtually entirely of the α modification. The α spherulites formed in such a density that there would be very little volume of material that would not be contained within a spherulite. Therefore, there is no second phase to make up for the less deformable α spherulite. However, it appears that a small number of spherulites get destroyed as the shear strain increases, and these regions are likely to make up for the lack of deformation of the intact α spherulites.

Looking along the LD and FD directions at a shear strain of 1.5 a spherulitic morphology still exists. A fibrous texture has been observed in other semicrystalline polymers, which have been subjected to shear deformation[13,18,22] and has been attributed to the formation of macrofibrils with their long axis aligned along the major tensile axis.[20] In agreement with these observations, in the present case a fibrous structure is observed looking along TD. These results can be explained if the spherulites are elongated into penny-shaped disks with their planes aligned along TD. It is expected that at increased shear strain the spherulite morphology looking down LD and FD will be destroyed as the pennies get elongated to such an extent that all of the inner fibrous structure of the spherulite gets elongated along the major tensile axis.

Shear Deformation on the Molecular Scale. At all shear strains investigated ($\gamma = 0.1-3.1$) a bimodal orientation of both the crystallites and molecular chain axis was observed. The angle of the preferred crystallite orientations appears to be similar to that found in SAXS patterns in PET[1820] at the shear strains investigated. In that work the scattering from the preferred orientation was thought to be due to the periodicity of successive lamellae. In this research, simultaneous WAXS and SAXS measurements reveals that the molecular *c*-axis is aligned along the C_2 crystallite plane and nearly aligned along C_1 planes until high shear strains are attained. As the chain axis is contained in or near the plane of the crystallites, the observed scattering therefore cannot be due to lamellar scattering, as suggested above. The observed scattering also cannot be due to any parent−daughter effects as similar bimodal distributions are observed in other polymer systems which are not known to form parent−daughter structures, such as PET and HDPE. The most likely structure which fits this structure is therefore a microfibrillar one analogous to that formed during cold drawing.

The sequence of morphological changes observed during shear deformation closely parallels that observed during tensile deformation of iPP by Balta-Calleja and Peterlin,[48] where the transition from the spherulitic to the fiber structure occurs as the material passes into the necked region during the cold-drawing process and is associated with the material undergoing plastic yielding. Like the present work it was noted there was a near continuous transformation from the spherulitic to the final fiber structure. It was proposed that microfibrils form discontinuously at numerous micronecks distributed randomly throughout the whole neck area of the tensile specimen. As the draw ratio increases, these microfibrils form the basis of the final fiber structure.

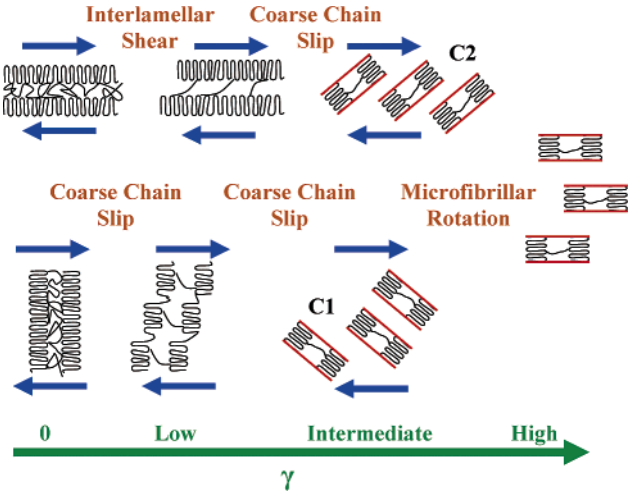

Figure 11. Formation of the two preferred microfibrillar orientations by simple shear deformation.

From the results obtained, the following model for the origin of the two preferred orientations is proposed on the basis of the initial orientation of lamellae within the spherulite (Figure 11). Chain slip is more likely to occur parallel or perpendicular to the molecular chain axis. Chain-folded lamellae whose planes are initially aligned along FD will undergo a small amount of interlamellar shear before the tie molecules between successive lamellae get completely stretched. This small amount of interlamellar shear is due to the high crystallinity of the polymer as well as the previously discussed interlocking nature of the parent−daughter structure, resulting in relatively few tie molecules between lamellae. After the tie molecules are completely stretched, further deformation can only be accomplished by coarse chain slip and the lamellar blocks sliding past one another. Fragmentation of lamellar blocks has previously been observed in iPP subjected to simple shear.[3] The principal tensile (and compressive) axis at this strain is inclined 43° to FD, and therefore the fragmented blocks will tend to initially align along it. This results in the first preferred orientation, C_2.

The second preferred orientation, C_1, is due to lamellae whose planes were initially oriented perpendicular to FD. In this orientation, interlamellar shear is not likely to be significant, and coarse chain slip will occur at very small shear strains. This was seen in the lower crystallinity of this preferred orientation compared to C_2. The fragmented blocks then get aligned along the maximum compressive axis. Lamellae whose normals were initially aligned along the principal tensile and compression axes will undergo interlamellar separation and contraction and will therefore not contribute to the observed preferred orientation.

With increasing shear strain, the orientation of both microfibrillar domains rotate toward FD and their relative concentrations increase. A possible reason why they do not stay aligned with the principal tensile and compressive axes is due to the original location of successive tie molecules being either parallel or perpendicular to FD. These tie molecules will tend to stay aligned horizontal or vertical, and therefore the entire fibrillar domain will rotate toward FD to accommodate the deformation. As deformation increases more lamellae are favorably oriented for chain slip, resulting in the increase in the relative concentration of both microfibrillar domains. C_1 microfibrils traverse a much wider arc than C_2 microfibrils which lead to it having a higher population.

Conclusions

Using the "less than ideal" properties of the ECAE process (as applied by us to polymers), varying degrees of simple shear

where able to be created in a semicrystalline sample of iPP. This allowed the following conclusions to be drawn about the evolution of morphology from low to high shear strains.

With increasing deformation the ribbons which make up the spherulite were elongated if they are aligned roughly along the major axis of the deformation ellipse while those aligned along the minor axis are destroyed, to be replaced with macrofibrils aligned along the direction of maximum tensile strain.

For all shear strains studied, and while the spherulite structure was intact, the deformation of the spherulite was found to lag ~20° behind the overall (macro) deformation. This was thought to be due to the interlocking nature of the α spherulites stiffening them against deformation.

Two preferred crystallite and molecular *c*-axis domains were observed in both WAXD and SAXS patterns. Both preferred orientations were observed at the lowest shear strain investigated, $\gamma = 0.1$, revealing that only small shear strains are required to cause a radical change in morphology.

In both preferred orientations the chain axis was observed to be incorporated along the length of the crystallite, and therefore the observed SAXS scattering cannot be due to lamellae scattering. It is proposed that the observed scattering is due to microfibrils analogous to that found in cold drawn samples.

A mechanism for the formation of the two preferred microfibrillar orientations was proposed on the basis of the initial orientation of a lamella to the shear direction. Lamellae whose planes were initially oriented perpendicular to FD lead the formation of C_1 microfibrils whereas lamellae whose planes are initially aligned parallel to FD lead to the formation of C_2 microfibrils.

Acknowledgment. This work was performed at the Australian National Beamline Facility (ANBF) with support from the Australian Synchrotron Research Program, which is funded by the Commonwealth of Australia under the Major National Research Facility Program. Dr. James Hester (ANBF) is gratefully acknowledged for his assistance in the experiments.

References and Notes

(1) Castelein, G.; Coulon, G.; G'Sell, C. *Polym. Eng. Sci.* **1997**, *37*, 1694−1701.
(2) Bartczak, Z.; Argon, A. S.; Cohen, R. E. *Polymer* **1994**, *35*, 3427−2441.
(3) Coulon, G.; Castelein, G.; G'Sell, C. *Polymer* **1998**, *40*, 95−110.
(4) Lee, B. J.; Argon, A. S.; Parks, D. M.; Ahz1, S.; Bartczak, S. *Polymer* **1993**, *34*, 3555−3575.
(5) Aboulfaraj, M.; G'Sell, C.; Ulrich, B.; Dahoun, A. *Polymer* **1995**, *36*, 731−742.
(6) Bartczak, Z.; Cohen, R. E.; Argon, A. S. *Macromolecules* **1992**, *25*, 4692−4704.
(7) Galeski, A.; Bartczak, Z.; Argon, A. S.; Cohen, R. E. *Macromolecules*, **1992**, *25*, 5705−5718.
(8) Bartczak, Z.; Galeski, A.; Argon, A. S.; Cohen, R. E. *Polymer* **1996**, *37*, 2113−2123.
(9) Lin, A.; Argon, A. S. *Macromolecules* **1992**, *25*, 4011−4024.
(10) Segal, V. M. *Mater. Sci. Eng.* **1995**, *A197*, 157−164.
(11) Segal, V. M. *Mater. Sci. Eng.* **1999**, *A271*, 322−333.
(12) Cronwell, L. R.; Hartwig, K. T.; Goforth, R. E.; Semiatin, S. L. *Mater. Charact.* **1996**, *37*, 295−300.
(13) Sue, H. J.; Li, C. K.-Y. *J. Mater. Sci., Lett.* **1998** *17*, 853−8566.
(14) Campbell, B.; Edward, G. *Plast., Rubber Compos.* **1999**, *28*, 467−475.
(15) Sue, H. J.; Dilan, H.; Li, C. K.-Y. *Polym. Eng. Sci.* **1999**, *39*, 2505−2515.
(16) Li, C. K.-Y.; Xia, Z. Y.; Sue, H. J. *Polymer* **2000**, *41*, 6285−6293.
(17) Xia, Z. Y.; Sue, H. J.; Hsieh, A. J. *J. Appl. Polym. Sci.* **2001**, *79*, 2060−2066.
(18) Xia, Z. Y.; Sue, H. J. *Macromolecules* **2000**, *33*, 8746−8755.
(19) Xia, Z. Y.; Sue, H. J.; Hsieh, A. J.; Huang, J. W. L. *J. Polym. Sci., Part B*: *Polym. Phys.* **2001**, *29*, 1394−1403.
(20) Xia, Z.; Hartwig, T.; Sue, H. J. *J. Macromol. Sci., Part B: Phys.* **2004**, *B4*, 385−403.
(21) Creasy, T. S.; Kang, Y. S. *J. Thermoplast. Compos. Mater.* **2004**, *17*, 205−227.
(22) Weon, J. I.; Xia, Z. Y.; Sue, H. J. *J. Polym. Sci., Part B: Polym. Phys.* **2005**, *43*, 3555−3566.
(23) Weon, J. I.; Sue, H. J. *Polymer* **2005**, *46*, 6325−6334.
(24) Aboulfaraj, M.; Ulrich, B.; Dahoun, A.; G'Sell, C. *Polymer* **1993**, *34*, 4817−4825.
(25) Zhu, P.; Phillips, A.; Tung, J.; Edward, G. *J. Appl. Phys.* **2005**, *97*, 104908 1−6.
(26) Zhu, P.; Tung, J.; Phillips, A.; Edward, G. *Macromolecules* **2006**, *39*, 1821−1831.
(27) Karger-Kocis, J. *Polypropylene. An A−Z Reference*; Kluwer Academic Press: Great Britan, 1999; p 57.
(28) Viana, J. C.; Cunha, A. M.; Billon, N. *Polymer* **2002**, *43*, 4185−4196.
(29) Olley, R. H.; Hodge, A. M.; Bassett, D. J. *J. Polym. Sci., Polym. Phys.* **1979**, *17*, 627.
(30) Olley, R. H.; Basset, D. C. *Polym. Commun.* **1982**, *23*, 1710.
(31) Park, J.; Eom, K.; Kwan, O.; Woo, S. *Microsc. Microanal.* **2001**, *7*, 276−286.
(32) Karger-Kocis, J. *Polypropylene. An A−Z Reference*; Kluwer Academic Press: Great Britan, 1999; p 608.
(33) Cunnif, P. M.; Phillips, R. A. *J. Mater. Sci.* **2001**, *36*, 3071−3077.
(34) Shaofeng, R.; Zong, X.; Fang, D.; Hsiao, B. S.; Chu, B.; Phillips, R. A. *Macromolecules* **2001**, *34*, 2569−2578.
(35) Butler, F. M.; Donald, M. A.; Ryan, A. J. *Polymer* **1997**, *38*, 5521−5538.
(36) Ruland, W. *Acta Crystallogr.* **1961**, *14*, 1180−1185.
(37) Kalay, K.; Bevis, M. J. *J. Polym. Sci., Part B: Polym. Phys.* **1997**, *35*, 265−291.
(38) Diez, F. J.; Alvarino, C.; Lopez, J.; Ramirez, C.; Abad, M. J.; Cano, J.; Garcia-Garabal, S.; Barral, L. *J. Therm. Anal. Calorim.* **2005**, *81*, 21−25.
(39) Lima, M. F. S.; Zen Vasconcellos, M. A.; Samios, D. *J. Polym. Sci., Part B: Polym. Phys.* **2002**, *40*, 896−903.
(40) Natta, G. *J. Polym. Sci.* **1955**, *16*, 143−154.
(41) Varga, J. *J. Mater. Sci.* **1992**, *27*, 2557−2579.
(42) Katti, S. S.; Schultz, J. M. *Polym. Eng. Sci.* **1982**, *22*, 1001−1017.
(43) Lotz, B.; Wittmann, C. J. *J. Polym. Sci., Part B: Polym. Phys.* **1986**, *24*, 1541−1558.
(44) Lin, L.; Argon, A. S. *J. Mater. Sci.* **1994**, *29*, 294−323.
(45) G'Sell, C.; Dahoun, A. *Mater. Sci. Eng.* **1994**, *A175*, 183−199.
(46) Peterson, J. M. *J. Appl. Phys.* **1966**, *37*, 4047−4050.
(47) Young, R. J. *Mater. Forum* **1988**, *11*, 210−216.
(48) Peterlin, A. *Plastic Deformation of Polymers*; Marcel Dekker: New York, 1971; pp 59−79.

MA0607618